Combined MA-XRF, MA-XRPD and SEM-EDX analysis of a medieval stained-glass panel formerly from Notre Dame, Paris reveals its material history

Combined MA-XRF, MA-XRPD and SEM-EDX analysis of a medieval stained-glass panel formerly from Notre Dame, Paris reveals its material history

Arthur Gestels[a,d*], Geert Van der Snickt[a,b], Joost Caen[b], Gert Nuyts[a], Stijn Legrand[a,b], Frederik Vanmeert[a,c], Flore Detry[b], Koen Janssens[a,b], Gunther Steenackers[d]

[a.] *University of Antwerp, Department of Physics, AXIS research group, Groenenborgerlaan 171, B-2020 Antwerp, Belgium.*
[b.] *University of Antwerp, ARCHES research group, Mutsaardstraat 31, B-2000 Antwerp, Belgium.*
[c.] *Royal Institute for Cultural Heritage, Laboratory Department, Jubelpark 1, B-1000 Brussels, Belgium.*
[d.] *University of Antwerp, InViLab research group, Groenenborgerlaan 171, B-2020 Antwerp, Belgium.*
**Corresponding author at: AXIS Research Group, Department of Physics, University of Antwerp, Groenenborgerlaan 171, B-2020 Antwerp, Belgium.*
E-mail address: arthur.gestels@uantwerpen.be (A. Gestels).

Abstract

As part of its conservation-restoration, the 13th century stained-glass panel 'the Annunciation', was examined at the micro- and macro level. This window, since 1898 in the collection of the *Museum Mayer Van den Bergh* (Antwerp, B), was formerly a part of the southern Rose window of the Notre Dame Cathedral (Paris, F). The insigths emerging from a first phase of the analysis, comprising non-invasive analysis techniques such as optical microscopy combined with macroscopic X-ray fluorescence (MA-XRF) and X-ray diffraction (MA-XRPD) mapping, were used to select sampling positions for the second phase of investigation that involved micro-invasive analysis, namely scanning-electron microscopy coupled to energy-dispersive X-ray analysis (SEM-EDX). The aim of the investigation was fourfold: (1) to assess the applicability of MA-XRF scanning for the characterisation of stained glass windows prior to any conservation or restoration procedure, (2) to assess the applicability of MA-XRPD scanning to identify the degradation products formed on the surface of stained glass windows, (3) to establish a method to limit the set of sampled glass fragments taken from a glass panel for quantititive analysis while maintaining sufficient representativeness and (4) to distinguish the original glass panes and grisaille paint from non-original glass panes that were inserted during various past interventions. Most of the panes in this window proved to consist of medieval potash glass, consistent with the 13th c. origin of the window while a limited number of panes were identified as non-original infills, with divergent glass compositional types and/or colorants. Most panes derive their color from the pot metal glass (i.e. homogenously colored) they were made of. Some of the panes that originally had a red flashed layer on their surface, completely or partially lost this layer due to weathering. Three main compositional glass families with similar color could be defined. With the exception of the yellow and orange panes, the chromophoric elements responsible for the dark(er) and light(er) blue (Co), green (Cu), purple (Mn) and red colors (Cu) were identified. Two different grisaille paints were encountered, part of which were restored during the 19th century. On the basis of this information, all missing pieces were replaced by glass panes with appropriate colors and the panel could be successfully conserved to its former glory. On the surface of several panes, typical glass degradation products such as calcite, syngenite and gypsum were identified, together with lead based degradation products such as anglesite and palmierite. In addition, the presence of hematite and melanotekite in the grisailles was observed; also the presence of Zn, uncorrelated to Cu, in the grissailes on the right side of the window became apparent.

Keywords

Stained-glass; Chemical imaging; MA-XRF; SEM-EDX; MA-XRPD; Glass composition

1. Introduction

Stained glass windows are prevalent in church buildings from earlier than 1000 A.D. to the present day and therefore constitute an important part of religious and cultural heritage. Traditionally, the material history of a medieval stained glass panel is derived by a combination of archival research and visual examination, optionally augmented with chemical analysis of the individual glass panes constituting the panel. In literature, a wide range of techniques have been surveyed for glass analysis; most established methods are X-ray fluorescence (XRF) and scanning electron microscopy equipped with energy dispersive X-ray detection (SEM-EDX).[1-4] Both methods owe their popularity to the ability of detecting and quantifying a wide range of elements in a sensitive and efficient way.[5, 6] The principal reasons why such information is relevant is that (a) during the course of its history, individual glass panes of a stained glass window may gradually become replaced by non-authentic equivalents with another (elemental) composition and (b) during their age-long exposure to the (indoor and/or outdoor) environment, especially the glass paints use to stain the glass may suffer from severe degradation. In the past, the authors demonstrated the relevance of Macroscopic X-ray fluorescence (MA-XRF) mapping as non-invasive elemental imaging method for stained glass panels.[7, 8] The major benefit of MA-XRF was identified as its ability to acquire compositional data from the entire surface in a completely non-destructive way, an aspect that was highlighted by the discovery of an enigmatic cobalt-based green glass in a well-studied stained glass window of exceptional quality. In addition, the ensuing chemical data can be presented in a visual way, hence allowing interpretation by non-

XRF specialists. Other non-invasive techniques such as UV-VIS and Raman spectroscopy are also frequently used in the analysis of stained glass windows. Uv-Vis-NIR spectroscopy is often used for the investigation of colored glass, moreover it can also be used for the distinction between different glass compositions.[9, 10] In-situ Raman spectroscopy can also be used discriminating between different glass compositions.[11] An advantage of MA-XRF over the aforementioned techniques is that MA-XRF cannot only identify the chromophores in the glass. It also allows to distinguish between pot metal glass (chromophores present throughout the entire glass plane) and flashed glass (chromophores only present in a thin sliver of coloured glass on top of uncoloured substrate glass). However, in contrast with conventional SEM-EDX and µ-XRF point analyses on minute glass samples, MA-XRF does not allow for accurate quantification of the different glass components; the absence of absolute concentration data prevents inter-comparison of MA-XRF data obtained from different stained-glass windows. In this respect, combining qualitative/semi-quantitative MA-XRF mapping with quantitative SEM-EDX analyses on a limited number of samples was expected to be highly relevant. Recently, Bracci et al. and Van der Snickt et al. integrated the use of non-invasive (VIS range hyperspectral imaging and MA-XRF) and micro-invasive analysis techniques (SEM-EDX) for stained glass artefacts; the main advantage of such a combination is that the number of glass panes that need to be sampled can be kept to a minimum while maintaining the representativeness of the analysis.[8, 12]

In the investigation of stained glass windows, X-ray powder diffraction (XRPD) is a technique that can be used to investigate crystalline compounds that precipitated on the surface or in the bulk of glass.[13, 14] Mostly, it is used to identify the formed crystalline compounds in the grisailles or the degradation products.[15, 16] However to the best of our knowledge, this is the first study that uses a mobile XRPD scanner for the analysis of stained glass windows.

In this work we employ a combination of several non-invasive and micro-invasive methods to trace the material history of a 13th c. *Annunciation* panel (diameter 50.1 cm) that currently belongs to the collection of the *Museum Mayer van den Bergh* in Antwerp, Belgium. This medieval stained glass window of exceptional quality was analyzed as part of its conservation-restoration process. Next to being used for their own merits, the results of the non-invasive imaging are employed to select and motivate the location of a minimal set of sampling locations on the multicolored glass window.

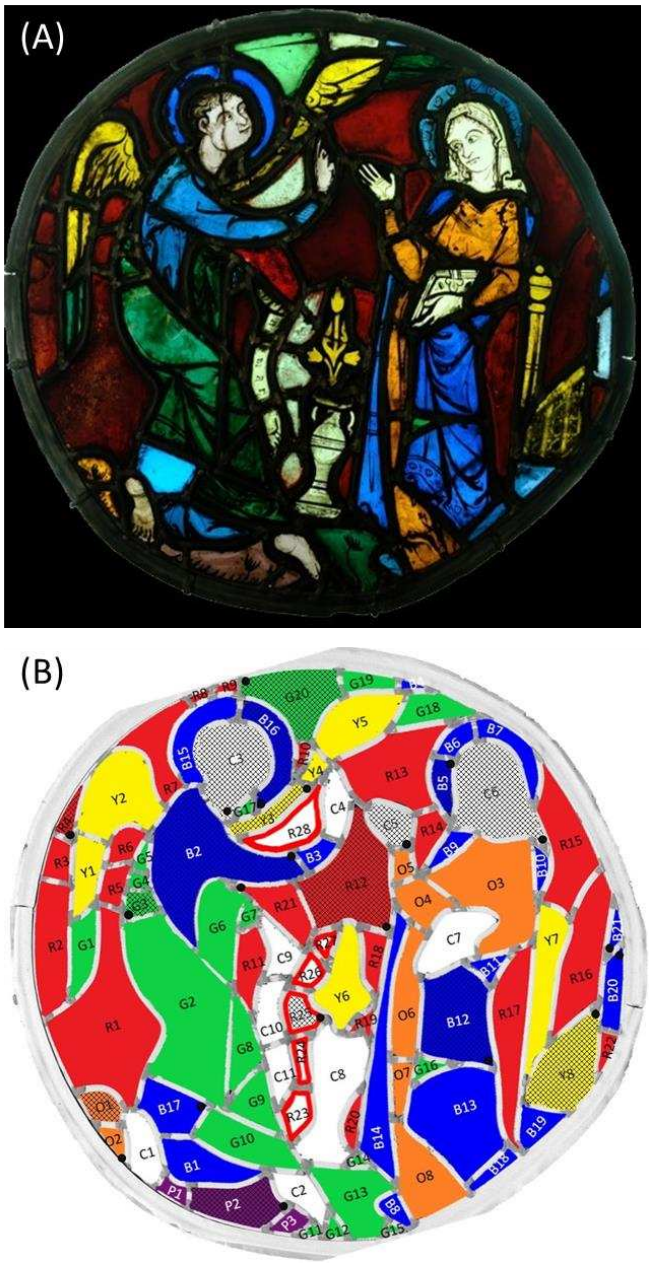

Figure 1. The Annunciation Window, *Museum Mayer van den Bergh*, Antwerp, Belgium (diameter: 50.1 cm) before the restoration treatment of 2020. (A) Visual photograph in transmitted light; (B) scheme with coded glass panes, the colors indicate the visual color of the glass. Black dots indicate the locations of samples discussed in table 1. The cross-hatched panes were identified as potash glass by means of the SEM-EDX analysis.

2. Material history

The investigated stained-glass window shows a classical Annunciation scene with the archangel Gabriel on the left, informing the virgin Mary that she is to bear a son. This message from heaven is symbolized by the scroll (in colorless glass) to the right of the angel. Also a vase (colorless glass) with three lilies (yellow glass), symbolizing the trinity, and a piece of furniture (a *prie dieu,* yellow glass) are visible. The dominant color of the background is red; the angel's garb consists of blue and green panes while Mary's clothing contains orange and blue elements. The panes representing the haloes of both figures are blue. The faces of Mary and Gabriel are in colorless glass, but that of Gabriel is slightly pinkish. A number of anatomical and other details have been rendered using grisaille paint.

Archival research revealed an intricate provenance and material history. This panel was once part of the large rose window in the southern transept façade (built between 1258 and 1260) of the *Cathédrale Notre Dame* in Paris, France (Figure 2B). However, historical textual sources indicate that it was not designed for this location and revealed an animated but fragmentary provenance. Although originally not conceived for the Notre Dame façade, scholars do situate the *Annunciation* panel in its vicinity on stylistic grounds. The range of glass colors, the simple composition with two characters, the uniform background, the slender S-shaped figures with elongated fingers and toes and the virtuoso but precise trace lines and shadows show a strong resemblance with other windows from *Ile de France* created between 1260 and 1280, such as the stained-glass windows in the *Saint-Sulpice* church in Saint-Sulpice-de Favières (Essonne, France) and panels in a private collection in the USA, originating from the church of Mantes-Gassicourt (Yvelines, France).
In the 1720s, the 13th c. south transept façade of the Notre Dame Cathedral was entirely rebuilt in response to instability of the stonework. Records indicate that the lead cames of the medieval stained-glass panels that were still in place at that time were re-leaded by Guillaume Brice, active in Paris between 1700 and 1737. The lead cames form a network of metallic lead profiles that hold the separate pieces of glass together. At this point, this renowned restorer of stained-glass panels filled the missing parts in the rose with coeval panels from his own collection, entirely in line with the prevalent restoration practices of that era. According to the 20th c. scholars Aubert, Perrot and Gatouillat, the panel studied here was one of the panels inserted by Brice in the rose window.[17-19]

In 1830, the rose window was again severely damaged by a fire and in 1861 architect Eugène Viollet-le-Duc rebuilt the instable façade once more. Stained-glass artist and art dealer Alfred Gérente was charged with the restoration of the rose window panels, and replaced at that occasion the *Annunciation* panel with a copy (Figure 2C). Between 1861 and 1895 the medieval panel entered the collection of Carlo Micheli, another Parisian artist and antique dealer, where it remained until the death of his wife in 1898. In that year, their entire collection, including the panel described here, was sold to the Antwerp art collector Fritz Mayer van den Bergh, whose collection formed the basis of the current museum.

Since the opening of the museum in 1904, the panel was presented in the 'grand gothic room' of the *Museum Mayer van den Bergh* (MMVDB).[20] In 1972, the architecture of the museum was modernized during which the panel most likely underwent an (undocumented) intervention. After being re-leaded, the panel was installed against a window of the 'little gothic room' at the first floor of the museum where it remained until the recent (2020) treatment. In 2018, the panel was declared 'National Treasure of Flanders' ("Vlaams topstuk"), a status guarantying special protection of the item and inducing an in-depth conservation-restoration treatment. As part of this treatment the panel has been thoroughly examined and chemically analyzed in 2020-2021, with the ensuing results described below.

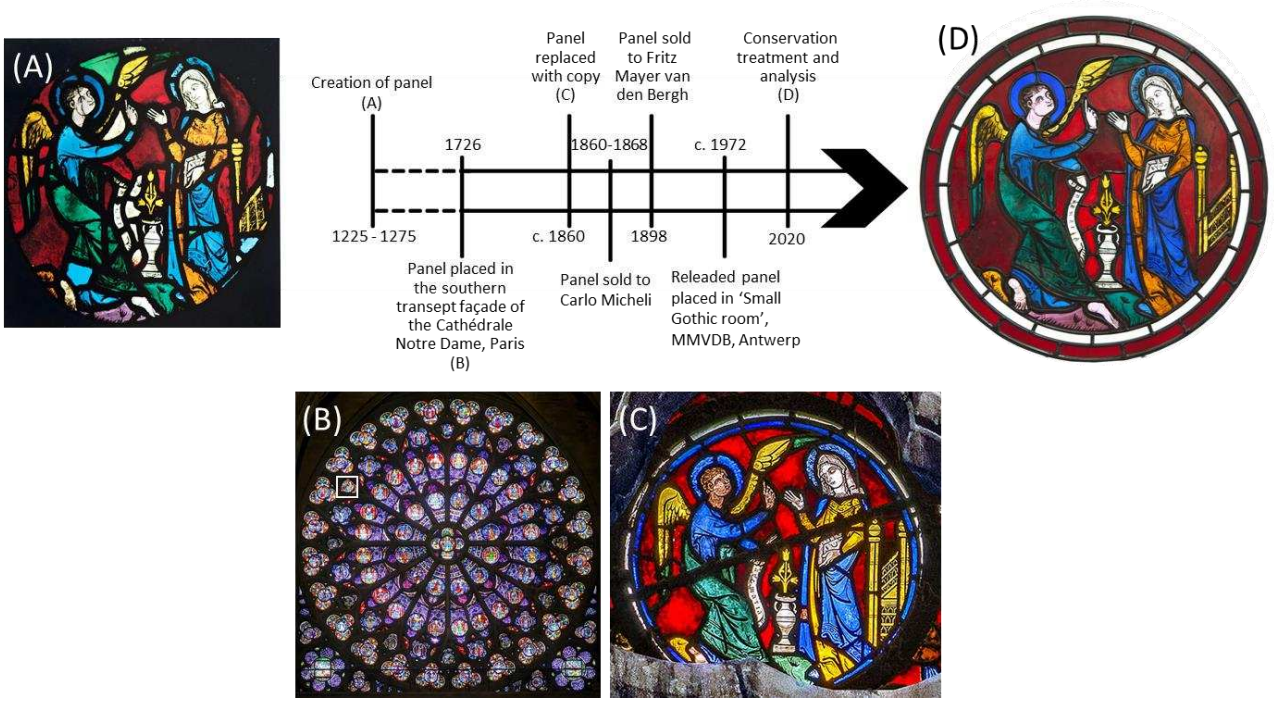

Figure 2. Timeline of the Annunciation panel: (A) photograph of the Annunciation panel published in the portfolio of J. Helbig, prior to releading of 1972, (B) interior view of the rose window, with the white rectangle indicating the location (of a copy) of the panel (situation prior to the 2019 fire), (C) interior view of the copy of the Annunciation panel currently in the rose window, (D) The Annunciation window in its present form, after the restoration of 2020.

3. Experimental

In preparation of the conservation treatment, the panel was visually examined in detail with support of optical microscopy. In the next phase, the panes of the glass window were non-invasively analyzed by means of Macroscopic X-Ray Fluorescence. During the conservation treatment, and after the glass panes were removed from the lead came network multiple panes were analyzed by means of Macroscopic reflection X-Ray Powder Diffraction (MA-rXRPD) imaging. A limited number of glass micro-samples were collected based on the results of the preliminary analyses. The micro-samples were characterized by means of a Field Emission Gun Environmental Scanning Electron Microscope equipped with an Energy Dispersive X-ray spectrometer (FEG-ESEM-EDX).

3.1 MA-XRF

The *Annunciation* panel was chemically imaged by means of an in-house built mobile MA-XRF scanner (AXIS, University of Antwerp, Belgium).[21] The device uses a 50-W XOS fleXBeam micro tube with Rh anode (XOS, USA) operated at 50 kV and 1 mA and one Vortex EX-90 SDD detector with an active area of 50 mm^2 positioned at 45° relative to the surface normal. The excitation beam was normal to the glass surface and was focused to a focal spot of ca. 200 µm by means of a polycapillary x-ray lens. This XRF measurement head was mounted on a software controlled X–Y motor stage with a maximum travel range of 57 × 60 cm (h × v). MA-XRF scans were performed by sweeping the measuring head systematically over the glass surface. Careful positioning and alignment of the scanner ensured a stable distance of ca. 2.25 cm in between the snout of the measuring head and the panel. Keeping this distance constant reduces fluctuations of the X-ray fluorescence signal by attenuation in the ambient air. During movement, XRF spectra were recorded in reflection mode every 500 µm (step size) with a dwell time of 207 ms and 215 ms for the internal and external side of glass panel respectively. The resulting spectral data cube was processed employing a combination of Pymca and Datamuncher software packages.[22, 23]. The MA-XRF measurements were performed at the start of the conservation process.

3.2 MA-XRPD

The MA-XRPD measurements were performed by means of an in-house built mobile scanner (AXIS, University of Antwerp, Belgium). The device is set-up with a low power X-ray micro source (50W, IµS-Cu, Incoatec GmbH, Germany), which produces a monochromatic and focused X-ray beam (Cu–K_α; 8.04 keV), a more detailed description can be found elsewhere.[24] A primary beam angle of incidence of 10° relative to the glass surface was employed due to geometrical limitations. This caused the beam footprint to become elongated in the horizontal direction so that it was of the order of 0.8 mm in the horizontal and 0.2 mm in the vertical direction. A PILATUS 200K area detector was used to record 2D diffraction patterns for each irradiated position. To reduce the effect of local topography and curvature of the glass surface on the diffraction data, the distance between the artwork and the scanner was automatically adjusted with a laser distance sensor (Baumer GmbH, Germany) at each measurement point. All components are placed on a motorized platform that is capable of moving in the XYZ directions (30 x 30 x 10 cm^3). The in-house developed software package XRDUA was used for the processing of all XRPD data. XRDUA provides the necessary tools for extracting crystalline-specific distributions from the large number of 2D diffraction patterns obtained during XRPD imaging experiments.[25]

The MA-XRPD measurements took place after removal of putty remains from the edges of the glass panes and subsequent rinsing with a water/ethanol (50/50) mixture. The benefit of this cleaning process was that the panes were already removed from the lead frame and could be individually placed in front of the instrument. In some areas where the glass panes were severely weathered, pure ethanol was used; however much care was taken to avoid overcleaning/damage to the substrate glass. A selection of fragments was made to analyze the internal and/or the external pane surface by performing point or line scans.

3.3 FEG-ESEM-EDX

Very small fragments of glass were collected from a selected number of panes, on the locations indicated in Figure 1B (black dots). The glass samples were examined with a Field Emission Gun – Environmental Scanning Electron Microscope (FEG-ESEM) equipped with an Energy Dispersive X-Ray (EDX) detector (FEI Quanta 250, USA), using an accelerating voltage of 20 kV, a take-off angle of 30°, a working distance of 10 mm and a sample chamber pressure of 10^{-4} Pa. Imaging was performed based on secondary (SE) and back-scattered electrons (BSE). EDX spectra from specific locations and regions of the glass were acquired, using a beam current of ~0.5 nA and a dwell time of 60 s per spectrum. The same beam current was used for EDX mapping. All maps were recorded with a resolution of 1024 by 704 pixels, with pixel sizes of 0.2-0.5 µm, and a dwell time of 0.5 ms per pixel. All EDX data analyses were performed by using the Aztec software package (Oxford Instruments).

4. Results & discussion

The MA-XRF maps shown in Figure 3 were recorded from both the internal and external sides of the panel with the aim of shedding light on the various interventions that were signaled by the aforementioned archival research. This was done prior to the actual start of the conservation process, i.e. with the glass panes still framed by the lead came network. Some of the ensuing elemental distribution images reveal relevant information on a number of important technical aspects of the window: the major glass constituents (Si, K and Ca) as well as some relevant trace elements (Rb, Sr, Ba, Ti), colorants (Cu, Co), opacifiers (Sn) and decolorizers (Mn and As) that are present in the glass. Other elemental maps provide information on the glass paints (Fe, Cr, Co) or the lead came network and its soldering (Pb, Sn). As is visible in Figure 3 K and L, in some areas, the glass of the panes was broken while cracks were filled with a Ba- and Sr-rich material (possibly a putty or glue mixed with $BaSO_4$ and/or $SrSO_4$). The XRF spectra recorded in these areas display Ba and Sr peaks with particularly high intensity and were excluded from the correlation plots of Figure 4A and B, discussed further in the text, to facilitate making the distinction among clusters caused by variations at trace level. The presence of barite ($BaSO_4$) was confirmed by means of MA-XRPD inside a crack in Gabriel's wing.

A full set of all elemental maps and the XRF sum spectra resulting from the MA-XRF scans can be found in the supplementary information (Figures SI1 and SI2) whereas their interpretation is discussed below. The MA-XRF distributions for a given element derived from both faces of the window are often dissimilar; the different reasons for this are discussed more in detail below. Since on most panes, the grisaille is present on the interior side, the MA-XRF maps derived from the exterior side were preferred to gather information on the type, color and authenticity of the actual glass panes while the maps from the interior side were used to provide data about the glass paints present.

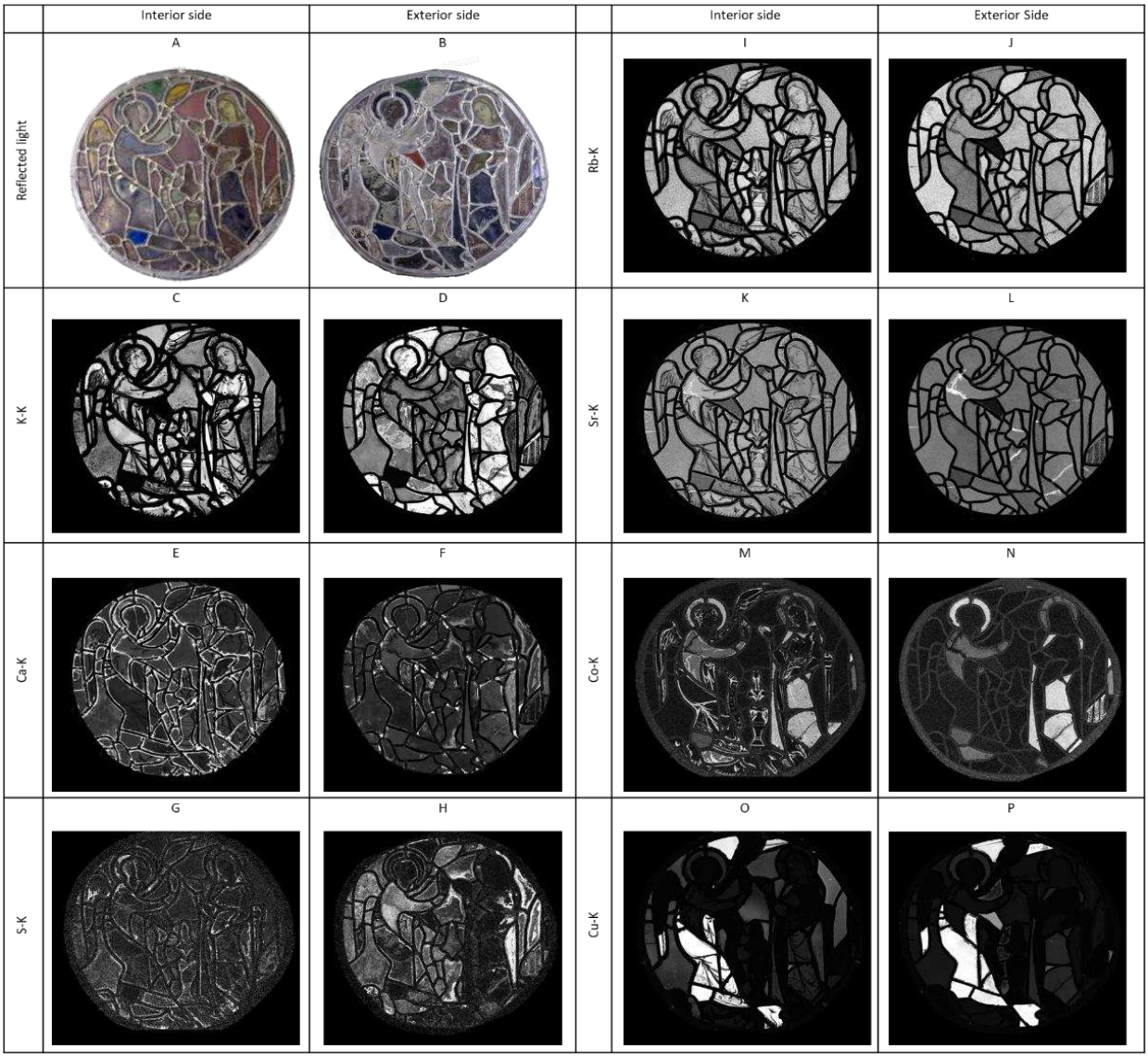

Figure 3. Reflected light photographs (A,B) and corresponding elemental distributions obtained by MA-XRF from the interior and exterior side of the window.

In Figure 1B, a false color scheme of the glass window with numbered and color-coded panes is presented to facilitate referring to all ninety-seven glass panes. G1 to G18 are the green colored glass panes, Y1-8 are yellow, B1-21 blue, C1-11 colorless, O1-8 orange, P1-3 purple and R1-28 red. In addition, the glass panes R23-28 are color coded in white with a red border to indicate that the original 'flashed' red glass-layer deteriorated over time, as discussed in more detail below.

On the basis of the MA-XRF data, various panes were first clustered into groups with similar substrate glass type, thus allowing to limit the number of glass samples required while still maintaining the representativeness of the quantitative dataset. In this way, minute glass samples were collected from a few panes belonging to each group. The resulting sampling locations of the glass samples for SEM-EDX micro analysis are indicated by black dots in Figure 1B . The corresponding quantitative data on the glass composition is presented in Table 1. As mentioned above, SEM-EDX analysis serves as a benchmark for the MA-XRF scanning results and at the same time complementary information can be gained leading to further insights into the properties of the stained glass.

4.1 Differentiating between glass types

As the chronological variation of glass composition in Western Europe is well-documented in literature, chemical analysis of the substrate glass within a stained window can be useful to recognize non-original panes that were introduced during past interventions. When available, quantitative compositional data can be used to cluster the panes in groups with similar glass type and (in favorable cases) place them in chronological order and link these to specific past intervention phases. All this can assist in reconstructing the often highly complex material history of a stained glass window.

As shown in previous studies, the added value of MA-XRF in this context is that data can be obtained from the entire glass surface, augmenting the representativeness of analysis.[8] For the specific purpose of distinguishing between panes of different glass types, the most obvious is to employ a correlation plot of the major elements Ca and K since the calcium and potassium content is indicative of respectively the network stabilizers and fluxing agent(s) present in the glass. However, as is evident from comparison of Figures 3B, D and F, the areas displaying prominent corrosion layers in the Annunciation panel, (such as the central part of panes G2 or G6) are visible as highlights in the Ca, K and S distribution maps, exhibiting signal intensities quite different from those in the areas with no or less degradation. As glass corrosion crusts often contain gypsum ($CaSO_4 \cdot 2H_2O$) and related materials, they result in a local increase of the detected Ca-K XRF signal and/or in an underestimation of the K-K signal due to shielding of the characteristic radiation stemming from the underlying bulk glass.

Nevertheless, the correlation plot of the Ca-K vs. the K-K peak intensities, collected from the exterior side and the corresponding composite false color image in Figure 4A, reveals several pixel clusters that can be associated with

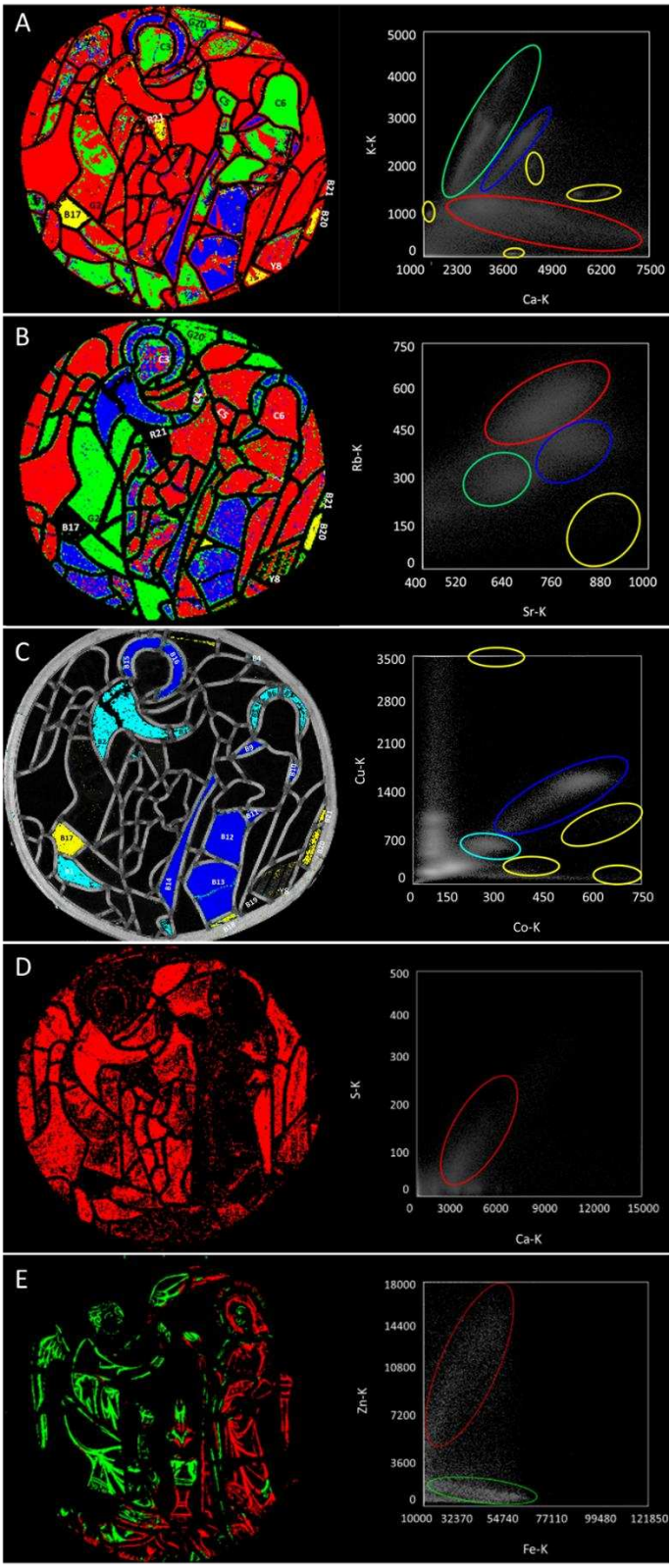

Figure 4. (A) (Ca-K, K-K) correlation plot and corresponding false colour pixel map based on MA-XRF data collected from the exterior side of the window. (B) Corresponding (Sr-K, Rb-K) correlation plot and false colour pixel map. (C) (Co-K, Cu-K) correlation plot and corresponding false colour pixel map. (D) (Ca-K, S-K) MA-XRF correlation plot and corresponding false colour pixel map of the exterior side of the window. (E) (Fe-K, Zn-K) correlation plot and corresponding false colour pixel map of the interior side of the window.

individual glass panes, suggesting that the large amount of data points (partly) evens out localized surface effects. In particular, the scatter plot shows (a) a group of pixels/glass panes that instantly stands out due to its high potassium signal (in false green), (b) a large cluster that is relatively poor in K, but richer in Ca (shown in false red in Figure 4A), (c) a group with intermediate values (in false blue) and (d) four separate sub-groups close to, but clearly distinct from the other clusters (in false yellow). The fact that several glass panes display pixels attributed to multiple groups is an effect of the presence of weathering crusts on the detected XRF signals (see above) and renders the interpretation of the results more difficult. This issue can be mitigated by plotting the XRF intensity of trace elements such as Sr and Rb that are typically associated with specific raw materials in the glass.[8] As reported in literature, the concentration of these trace constituents generally correlates well with the network stabilizer (chalk) and fluxing agents (potash and/or soda) respectively.[26-29] However, since Sr and Rb signals have more energetic X-ray fluorescence K-lines than K and Ca, their X-ray emission is less attenuated by the superimposed gypsum-like alteration layer. This reduced sensitivity to surface effects is evident when comparing the cluster maps of Fig. 4A and B. In general, the panes can be more firmly attributed to specific groups in the false color image of Fig. 4B. However, some ambiguities remain. For instance, the glass pane Y8 in Figure 4B shows some pixels belonging to the red and green clusters while most do not fall in any of the 4 labelled pixel groups. This misclassification is due to the fact that this pane was erroneously placed in reverse position during a previous intervention and therefore has glass paint on the exterior side of the window that affects the Rb-K to Sr-K ratio. In addition, two iconographical important panes, i.e. the face and the hand of the angel (C3-C4), cannot be clearly classified into either the green, red and blue cluster. The reasons for this remain unclear. It is not unthinkable that these panes are not infinitely thick at the Rb-K and Sr-K X-ray energies, a precondition for reliable clustering discussed in literature.[8] Apart from that, many panes display pixels along their edges that are not correctly classified; however, these are artefacts due to remnants of putty and/or to shadowing effects by the adjacent lead profiles.

Overall, the pixel clustering based on the Sr-K and Rb-K response confirms the previous clustering based on the Ca-K and K-K XRF intensities, with again three main clusters of which the most Ca-rich is shown in false red and the other two in false green and blue (Fig. 4B). Next to these, some panes with a deviating XRF response (such as B20, B21, G16) fall within the false yellow cluster while others (such as B17 and R21, both containing a lower amount of CaO and K_2O as seen in Table 1) show up black in Fig. 4B hence they fall outside all the aforementioned clusters. Compared to the (Ca-K, K-K)-based clustering, the attribution of some panes is now clearly revised.

sample	Colour	Glass Type	Na_2O	MgO	Al_2O_3	SiO_2	P_2O_5	SO_3	Cl	K_2O	CaO	TiO_2	MnO	Fe_2O_3	CoO	CuO	ZnO	SnO_2	PbO	K_2O/CaO
B16	blue	potash	0.4	4.9	1.7	50.9	3.7	<DL	0.3	17.0	18.0	0.2	1.2	0.9	0.2	0.3	0.5	<DL	<DL	0.93
B12	blue	potash	0.4	4.8	1.6	50.9	3.7	<DL	0.2	17.0	18.0	0.1	1.3	0.9	<DL	0.3	0.4	<DL	0.2	0.94
B5	blue	potash	0.8	4.4	1.9	45.9	5.8	<DL	0.1	20.0	19.0	0.2	1.1	0.8	<DL	<DL	<DL	<DL	<DL	1.04
B2	blue	potash	0.7	4.3	1.8	45.4	5.7	1.0	0.1	20.0	19.0	0.2	1.2	0.8	<DL	0.2	0.3	<DL	<DL	1.04
B17	**blue**	**soda**	**13.3**	**0.2**	**0.6**	**72.4**	**<DL**	**<DL**	**0.1**	**0.4**	**11.0**	**<DL**	**<DL**	**0.2**	**<DL**	**1.4**	**<DL**	**<DL**	**0.7**	**0.04**
B20	**blue**	**HLLA**	**0.2**	**3.2**	**1.4**	**64.5**	**1.8**	**<DL**	**<DL**	**7.6**	**19.0**	**0.2**	1.0	**0.5**	**<DL**	**<DL**	**<DL**	**<DL**	**<DL**	**0.40**
B21	**blue**	**HLLA**	**1.8**	**3.1**	**4.2**	**60.4**	**2.1**	**<DL**	**0.5**	**5.3**	**20.0**	**0.2**	**0.8**	**0.8**	**0.2**	**<DL**	**<DL**	**<DL**	**<DL**	**0.26**
R12	colourless	potash	0.4	4.5	1.7	48.6	4.9	0.3	0.2	20.1	17.3	0.1	1.3	0.5	<DL	<DL	<DL	>DL	<DL	1.16
R4	colourless	potash	0.4	4.5	1.6	48.4	4.9	0.3	0.2	20.3	17.5	0.1	1.3	0.4	<DL	<DL	<DL	<DL	<DL	1.16
R25	colourless	Potash	0.4	4.7	1.7	48.6	5.0	0.3	0.2	19.9	17.1	0.2	1.3	0.4	<DL	0.2	<DL	<DL	<DL	1.16
R25	red	potash	0.4	4.5	1.6	49.4	4.9	0.3	0.2	20.0	16.0	0.1	1.1	0.4	<DL	0.5	<DL	<DL	0.3	1.25
R4	red	potash	0.5	4.4	1.6	49.4	4.8	0.2	0.2	20.3	15.6	0.1	1.1	0.4	<DL	0.8	<DL	<DL	0.6	1.30
R12	red	potash	0.4	4.5	1.6	49.8	4.7	0.2	0.2	20.1	15.4	<DL	1.0	0.5	<DL	1.0	<DL	<DL	0.6	1.31
R21	**colourless**	**soda**	**14.1**	**0.3**	**0.3**	**74.0**	**<DL**	**0.2**	**<DL**	**0.1**	**11.0**	**<DL**	**<DL**	**<DL**	**<DL**	**<DL**	**<DL**	**<DL**	**<DL**	**0.01**
R21	**red**	**mixed/lead**	**4.1**	**0.2**	**0.3**	**56.9**	**<DL**	**<DL**	**0.6**	**9.4**	**6.5**	**<DL**	**<DL**	**0.9**	**<DL**	**1.4**	**<DL**	**5.5**	**14.2**	**1.45**
C6	colourless	potash	1.9	5.7	1.5	58.5	2.5	0.1	0.4	15.4	11.4	0.3	1.6	0.7	<DL	<DL	<DL	<DL	<DL	1.35
C5	colourless	potash	1.9	5.8	1.4	58.3	2.6	0.1	0.5	15.6	11.4	0.2	1.6	0.6	<DL	<DL	<DL	<DL	<DL	1.37
C3	light pink	potash	2.3	5.9	1.0	53.8	3.3	0.2	0.4	18.8	12.1	0.1	1.6	0.5	<DL	<DL	<DL	<DL	<DL	1.55
Y3	yellow	potash	0.3	4.2	1.7	47.2	3.8	0.3	0.2	24.3	15.9	0.2	1.4	0.4	<DL	<DL	<DL	<DL	<DL	1.53
Y8	yellow	potash	0.3	4.2	1.7	47.3	3.8	0.3	0.2	24.1	16	0.2	1.4	0.4	<DL	<DL	<DL	<DL	<DL	1.51
O2	orange	potash	0.4	2.8	1.6	49.8	1.3	0.4	0.1	25.9	15.9	0.2	1.2	0.3	<DL	<DL	<DL	<DL	<DL	1.63
G3	green	potash	2.0	7.0	1.4	50.0	4.5	0.2	0.4	18.1	12.3	0.2	0.9	0.7	<DL	2.3	<DL	<DL	<DL	1.47
G20	**green**	**potash**	**<DL**	**5.3**	**1.7**	**52.2**	**3.9**	**0.1**	**0.5**	**16.9**	**15.2**	**0.3**	**1.0**	**0.5**	**<DL**	**2.2**	**0.2**	**<DL**	**<DL**	**1.11**
P2	purple	potash	1.3	4.8	1.2	52.7	3.7	0.1	0.5	20.6	12.4	0.1	2	0.6	<DL	<DL	<DL	<DL	<DL	1.66

Table 1. Compositional data (in % m/m) obtained by SEM-EDX from the glass samples. All elements are quantified as their respective oxide. The location of the samples is indicated in Figure 1B. The results are grouped per color; data corresponding to later restoration panes are in bold. Cells with a diagonal in the column 'Glass type' indicate that the analysis was performed in the red stratum of a flashed glass pane. The uncertainy level of the quantitative data is estimated to be at the level of 1%.

Interestingly, the reviewed grouping based on trace elements comes close to a grouping based on color: the false color red group of Fig. 4B matches well with the red and colorless glass panes, the false green group matches the green glass and the false color blue group matches fairly well to the blue glass panes. In a previous study, similar observations were made for a late 15th c. *Saint Michael* panel from Bruges.[8] Also here, the red flashed panes were the richest in calcium, while the green glass emitted significantly higher potassium and lower calcium XRF intensities, approximately of the same order as uncolored glass.

In general, MA-XRF results were partly confirmed by SEM-EDX analysis. To facilitate the interpretation of the SEM-EDX quantitative compositions listed in Table 1, each analyzed glass sample was assigned a glass type following the hierarchical classification based on their major composition presented by Schalm et al.[30] Consistent with its 13th c. origin, most glass panes were found to consist of potash glass (with a K_2O content between 15 and 22% m/m). The samples taken from the three main MA-XRF clusters of Fig. 4B (red-green-blue) were all classified as potash substrate glass by SEM-EDX. The MA-XRF false yellow group and the panes shown in black in Fig. 4B corresponds with glass panes that were identified by the conservator as later infills, based on their divergent visual appearance and lower degree of corrosion. The deviating panes are made in distinctly different glass types: either high lime, low alkali glass (HLLA) (panes B20, B21), soda glass (panes B17, R21) or in a lead-rich mixed alkali glass (pane R21). The green pane G20 was visually also identified as a later infill as this pane would originally have been part of the red background. However, it was not recognized as non-original pane, neither by means of the MA-XRF clustering and on the basis of the SEM-EDX data. Instead, G20 was categorized as a potash glass, based on the classification method mentioned above. It is therefore difficult to differentiate G20 from the original panes based on the (Ca-K,K-K) and (Sr-K,-Rb-K) correlation plots. We therefore assume that G20 stems from re-use of old recycled glass, which was a common practice amongst glass restorers and is currently referred to as a 'stop gap'.[31, 32] The visual examination also led to the discovery of what seems to be the remnants of a painted face on the exterior side of the green robe of the angel (pane G2). These facial features emerge in the K-K and Pb-L maps as well and again suggests the recycling of glass, either from an older window or (more likely) a window that was abandoned in the studio or of panes of which the firing failed. The detail photograph of this pane can be found in SI3.
Summarizing, we can state that MA-XRF was able to reveal three distinct pixel clusters/pane groups, corresponding to historical, and likely original, potash glass types, and was able to detect infill panes made in glass with significantly different composition.

4.2 Glass colors

Since MA-XRF allows to record spatial distribution maps of chemical elements, imaging of chromophoric metal ions/atoms such as Cu^{2+} (for green glass), Cu^0 (as nanoparticles in red glass) and Co^{2+} (blue glass) is possible. Furthermore, the distinction between pot metal glass and flashed glass panes can be made in a straightforward manner upon comparing the elemental images recorded from both sides of the panel. Pot metal glass is homogenously colored throughout its entire thickness and the distribution of the coloring metal will therefore appear similar in the MA-XRF maps derived from both the interior and exterior side of the window. In case of flashed glass panes, where a thin layer of colored glass is applied on top of a (relatively thick) substrate of uncolored glass, the coloring metal ions will only be detected on a single side of the glass. However, previous studies have reported on the existence of more complex types of flashed glass, including those consisting of multiple colored strata and/or where the colored layer is covered by a so-called protective 'coperta' layer of uncolored glass.[33] In the following paragraphs, the detected metal ions are discussed in more detail.
In the Cu-K distribution (Figure 3 O and P), the green glass panes instantly stand out, exhibiting elevated copper signals along both sides of the window, while the red panes show up with lower average Cu-K signals, mainly along the interior side. This indicates that the green glass is of the pot metal type, colored by the introduction of Cu^{2+} ions into the glass batch in an oxidizing furnace atmosphere.[34] For the red glass, Cu is present as nanoparticles of metallic copper that dispersed in the flashed layer on the interior side.[33] The latter is consistent with the tradition of stained-glass artists to orient the thin red layer of flashed panes towards the interior where it is less prone to weathering. However, in the Annunciation window, a number of flashed pieces were clearly placed inside out. The red glass panes R21 and R22 show intense copper signals along the exterior instead of the interior side. In addition, in a second group of reversed panes (R23-28) the flashed layer clearly delaminated due to weathering, leaving only remnants of the red stratum along the edges/below the lead cames on the exterior side.
Additionally, copper signals were detected in a number of the blue glass panes (B9-B18), in which the blue color is mostly due to cobalt ions in the bulk glass.[35] Moreover, two of the 21 blue glass panes are flashed glass and not pot metal glass: B19 has its flashed layer along the interior; in pane B18, the blue layer is on the external side of the panel .
When considering the (Cu-K, Co-K) correlation plot (Figure 4C), several clusters show up, with two of the groups matching two visual hues of the blue glass panes. In particular, the false blue cluster corresponds with the deepest blue panes of Mary's blue dress (B9-14) and the archangel's nimbus (B15-16), while the false cyan group matches the lighter blue panes of the archangel's garment (B1-B3) and Mary's nimbus (B5-B7). Based on the previous discussion, these panes are considered original 13th c. glass. Again, SEM-EDX appears to confirm the clustering found by MA-XRF. The samples taken from panes B2 and B5 (false cyan cluster, lighter blue, Figure 4C) show a lower silica content (ca 45% m/m) and somewhat higher soda content (ca 0.7-0.8% m/m) present

compared to samples B12 and B16 (false blue cluster, darkest blue outlook) containing 50% SiO_2 and ca 0.4% Na_2O. Table 1 also confirms the presence of higher concentration of Cu present in the samples from the blue cluster (samples B12 and B16).
In the blue panes B2, B5 and B12, cobalt is not detectable by SEM-EDX although MA-XRF clearly shows that this element is present. Being a strong chromophore only a limited amount of cobalt is needed to give the glass a (strong) blue hue,[36] its concentration is likely below the SEM-EDX detection limit (± 0.05 wt%). Recently, Hunault suggested that copper is not present as a chromophore in French 13th century blue panes, but as an impurity of the cobalt ore and can be associated to another impurity of this ore, namely Zn.[35] However, a (Cu-K, Zn-K) MA-XRF correlation plot (not shown) cannot be straightforwardly used to verify this because the Zn distribution is also affected by the presence of other Zn-containing materials (see below).
In contrast, the panes shown in Figure 4C as false yellow show a quite divergent (Cu-K, Co-K)-ratio, evidencing that each individual pane stems from different batches. Moreover, these pieces were already flagged as inset panes of a later date during the above discussion of the (Ca-K, K-K) and (Sr-K, Rb-K) plots. In this plot, the pixels in which only copper and cobalt were detected show up as vertical or horizontal clusters close to the axes and are associated with green pot metal glass and grisaille of pane Y8 respectively and were not color-labelled to improve the readability of the cluster map.
The six pixel clusters indicated in Figure 4C also show up in correlation plots of the typical contaminant metals of the parent Co-ore minerals. See Figure SI4 and SI5 for the (Co-K, Ni-K) and (Co-K, As-K) correlation plots. As shown by the As-K image, panes B17 and B21 are particularly rich in arsenic; the Co-K to As-K intensity ratio of pane B21 suggests a deliberate addition of arsenic to the glass, as was customary in high quality 18th and 19th century glass, rather than a contamination.[37] From the SEM-EDX data (Table 1), it is possible to identify sample B17 as 19th century soda-lime glass due to its high soda (>11 wt%) and low magnesium and phosphorous contents. Sample B21 is identified as HLLA glass, a glass type which was common from the end of the 15th century until the 19th century.[30] Here SEM-EDX was not able to determine any As and Ni oxides above the detection limit.
The SEM-EDX analysis of sample P2 does point to a high Mn content resulting in the purple hue; in the Mn MA-XRF maps also panes P1-P3 light up, indicating elevated Mn levels.
Analysis and the dating of the glass both exclude the use of yellow glass paint as yellow silver stain was introduced only at the end of the 13th century and no Ag was detected.[38, 39] Therefor it is likely that the yellow and orange hues are originating from the specific redox and/or co-ordination states of iron, manganese and sulphur,[35, 40] While it is possible that specific kiln conditions may have been applied to achieve the desired colour, little is known on the exact formation of medieval bulk yellow and orange glasses.

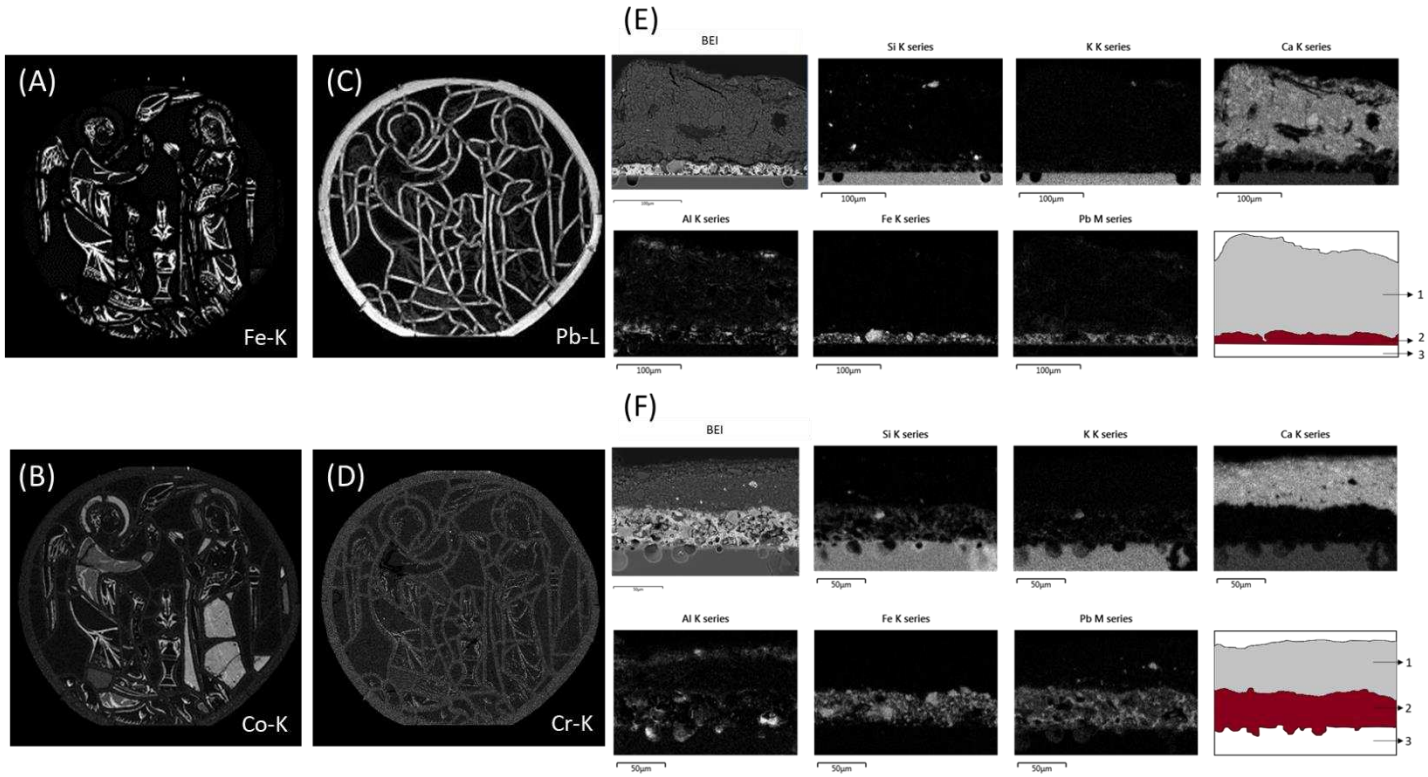

Figure 5. Selected MA-XRF maps from the interior side of the window: Fe-K (A), Co-K (D), Pb-L (C) and Cr-K (D). SEM-EDX maps of embedded cross-sections of glass samples taken from panels Y3 (A) and B5 (B). The schematic clarifies the 3-layered structure of these samples: putty layer (Ca-rich) (1), grisaille (rich in Pb and Fe) (2) and glass substrate (3).

4.3 Glass paints

At the assumed time of creation, grisaille was intensively used as an opaque glass paint for applying trace lines and shadowing on the individual glass panes. A grisaille consists of a glass powder mixed with metal oxide(s) and an organic binding medium to facilitate application and painting on the substrate glass, prior to firing. The paint is rendered opaque through the addition of iron oxides particles (such as hematite) or sulfates that do not dissolve in the glass melt. Lead oxides were commonly introduced to lower the glass melting point, allowing the paints to be fired without causing deformation to the substrate glass. Grisaille paints were predominantly applied onto the interior side of the panes in order to protect the relatively vulnerable paint from outdoor conditions. Consistent with this, all grisailles are visible in the MA-XRF iron and lead distributions collected from the interior side of the window, as shown in Figure 5A and C. The presence of hematite was detected by means of MA-XRPD in the grisailles, together with melanotekite ($Pb_2Fe_2(Si_2O_7)O_2$), an iron lead silicate, which is formed during the grisaille firing process.[14] Interestingly, the grisaille is rich in cobalt as well while also a limited amount of chromium is detected (Figure 5B and D). The presence of these two elements suggests a 19th century (partly) repainting of the grisailles (likely by glass restorer A. Gerenté) as both these elements are not encountered in glass paints of the medieval period.[41] Visual inspection of the grisailles allows to differentiate between two grisaille colors: a brown one and a black one. SEM-EDX maps of samples taken from grisaille-covered panels Y3 and B5 (Figure 1B) are shown in Figure 5E and F. A relatively thin grisaille layer (labelled 2, 10-50 µm), rich in Fe and Pb, covers the glass (3). On top of this, an additional Ca-rich layer (1) is present, interpreted to be the remains of Ca-containing putty (see also Figure 3E) and not of the repaint grisaille. As the sampling of the glass fragments was done in areas underneath or near the lead cames, as expected, no repainted grisaille layers (these were only applied in areas showing visible degradation) were encountered on the surface of these glass samples.
Upon inspecting the MA-XRF maps collected from the exterior side (Figure SI2), it becomes clear that the Y8 pane (the 'prie dieu') was erroneously placed in reverse position during a previous intervention and therefore featured glass paint on its exterior side.

4.4 Glass corrosion and superficial deposits

The exterior side of the *Annunciation* panel shows several forms of weathering. In reflected light, the external surface displays a whitish crust that is not uniformly distributed (Figure 3B). Glass weathering products are usually caused by an ion exchange between H^+-ions in water absorbed on the original glass surface and Ca^{2+} and/or K^+-ions that are leached out of the glass.[2] The latter can react with atmospheric compounds or species dissolved in the fluid in contact with the glass, forming carbonates, sulphates, chlorides and nitrates of the leached ions as well as organic compounds.[42-44] A detailed description of glass degradation mechanisms and the structural changes inside the glass it may cause can be found elsewhere.[45] The most commonly found corrosion crusts on medieval stained glass include the sulphates gypsum ($CaSO_4{\cdot}2H_2O$) and syngenite ($K_2Ca(SO_4)_2{\cdot}H_2O$). When looking at Figure 3H, it becomes apparent that the S-distribution is very similar to the shape of the crust, suggesting that one or more sulfate salts precipitated on the surface of glass window. The correlation plot of Ca-K and S-K shown in Figure 4D also suggests that calcium sulfates precipitated on the glass surface. Non-invasive MA-XRPD experiments of which the full overview is given in Table SI1, identified crystal phases typical of glass degradation: both calcium sulphates, gypsum and syngenite are present. Other calcium based degradation products were also identified: calcium carbonate (calcite, $CaCO_3$) and calcium oxalate (weddellite, $CaC_2O_4{\cdot}2H_2O$). The presence of oxalates can be attributed to the vital processes of micro-organisms (fungi, lichen and bacteria).[46, 47] Literature describes how the oxalic acid segregated by such micro-organisms can transform calcite into calcium oxalate.[48] Furthermore, lead-based degradation products such as palmierite ($K_2Pb(SO_4)_2$) and anglesite ($PbSO_4$) were found with MA-XRPD. These can be associated with glass paints and/or can result from reactions of environmental species with the lead cames. Furthermore, it is known that during degradation processes, environmental divalent cations such Pb^{2+} and Mn^{2+}, can enter cation-depleted glass corrosion bodies and precipitate there.[49, 50]
On the surface of the deep blue and orange glass panes, and especially on the panes constituting the Virgin Mary, a significantly thinner precipitation crust is visible. Throughout the panel, pit corrosion is present (Fig. Si6). SI6 shows that the corrosion pits show up in the Zn-K distribution of the external side of the window. On the other hand, on the interior side, the Zn-K distribution is related to the grisaille contour lines, especially on the right part of the window. The origin of this correlation remains unclear, but it is currently assumed that these are depositions of Zn-rich dirt or particulate matter from an external source. Zn-rich powdery material may have accumulated on the surface of the glass panes, and adhered on the surface especially in areas with a rough topography, such as areas with corrosion pits, grisaille paint or putty residues. Zn-compounds such as ZnO and ZnS are often used as a whitening agents in paints and other finishing layers, so it is not unthinkable that these are remnants released during construction works, painting or sanding of the museum interior. Interestingly, the (Fe-K, Zn-K) correlation plot shown in Figure 4E suggests that the glass panel can roughly be divided in two halves, each depicting one of the two figures. On the right side (Virgin Mary), a strong spatial correlation of Zn-K and Fe-K in the grisaille (false red cluster in Fig. 4E) suggests that hematite was used in the grisaille, which was also confirmed by means of MA-XRPD as mentioned earlier; here the positive correlation could be explained by assuming that traces of Zn are present in the hematite. To the best of our knowledge, in the past, Zn-containing grisaille was only found on two other occasions by Vilarigues et al.[49, 51] who suggested that the use of brass during the making of the grisaille

paints could explain the presence of Zn in the grisailles. However, in this case, no correlation could be found between the Zn and Cu distributions in the *Annunciation* window.
In the other half of the window (Archangel Gabriel), the negative correlation between the Fe-K and Zn-K (false green cluster in Fig. 4E) seems to be consistent with a Zn-containing covering layer (perhaps putty) that absorbs some of the Fe-K signals that originate in the grisaille layers underneath.

4.5 Result of the Conservation process

In Figure 2D, the *Annunciation* window is shown, after the finalization of the 2020-2021 conservation-restoration. Next to the replacement of the lead cames with thinner lead profiles and the addition of two outer borders of white and red glass panes, the putty and dirt remnants on the glass panes were removed. The broken panes, as for example the mantles of virgin and archangel were bonded together. Lacunae in the grisaille and the weathered red layer in some pieces of flashed glass were touched-up. Missing parts were reconstructed with modern glass of matching color and painted with grisaille paints. To make these additions easily visible, the trace lines and shades were highlighted with fine lines. Old infilling glass panes with unmatched colors, such as panels B17, G19, G20, were replaced by modern glass of appropriate colors. As part of the reconstruction of the *"prie dieu"*, the orientation of pane Y8 was switched around so that the grisaille paint is now on the interior side of the window. To reconstruct the chair, the inset glass panes R22, B20 and B21 were replaced by a painted yellow panel similar to original pane Y7 and Y8.
The conservator observed some particular aspects concerning the depiction of Mary. Compared with the other glass panes of the panel, all glass applied for the representation of Mary has special aspects. The glass of head and hands is quasi colorless and shows no corrosion. This in contrast to the head, feet and hand of the archangel Gabriel showing a pink-purple hue. From Table 1, it appears that there is also an analytical difference present between the panes depicting the heads of Mary (C5-C6) and Gabriel (C3). C5 and C6 contain a higher amount of SiO_2 than C3. The glass of Mary's blue coat is also of high quality and shows nearly no deterioration, whereas the orange glass of her dress, though weathered, is a rare color in Medieval (and later) stained-glass windows. All this suggests that the artist-glass painter took special care of the choice of materials when he realized the representation of Our Lady. A phenomenon that we also know from paintings and polychrome sculpture, but, as far as we know, never evidenced in stained glass.

5. Conclusions

In this paper, the material history of a corroded medieval stained-glass panel showing an Annunciation scene is revealed. In this regard, combining the information provided by the MA-XRF maps from both sides of the window with MA-XRPD and SEM-EDX analyses of a limited number of samples was particularly relevant. The fact that the non-invasive MA-XRF analysis was conducted prior to invasive sampling made it possible to select the sampling locations in an optimal manner while the number of samples needed for obtaining a comprehensive compositional overview could be minimized. The analyses led to the observation that among the 97 glass panes that constitute the panel, three different glass types were encountered: the original potash glass used in the 13th century, and two types present in restoration panes: HLLA and soda glass. With the exception of the yellow, orange and purple panes, the color of most pane colors could be attributed to the presence of one or more chromophoric ions. On the surface of several panes, typical glass degradation products were identified by means of a mobile MA-XRPD scanner, such as calcite, syngenite and gypsum, together with lead based degradation products such as anglesite and palmierite. The original grisaille paints can be visualized by the distribution of iron on the interior side of the window because of the presence of hematite in these paints; on the other hand, by means of the cobalt and chromium distributions, the extent of the 19th century restoration grisailles could be visualized. The XRPD measurements were able to confirm the presence of hematite and melanotekite in the grisailles.

Conflicts of interest

There are no conflicts to declare.

Acknowledgements

This research was part of the activities of the Chair on Advanced Imaging Techniques for the Arts, established by the Baillet Latour fund.
The authors acknowledge financial support from FWO Brussels through grant from FWO project: A combined IR, NIR and MA-XRF material inspection method with FWO ID G056619N and from Interreg Vlaanderen-Nederland (Smart*Light project).
Special thanks to the staff of the *Museum Mayer van den Bergh* (mmb@antwerpen.be) for this fruitful collaboration and authorization of the publication of the images, in particular Rita Van Dooren and Harlinde Pellens are acknowledged for their support.

References

1. Janssens, K.; Vittiglio, G.; Deraedt, I.; Aerts, A.; Vekemans, B.; Vincze, L.; Wei, F.; De Ryck, I.; Schalm, O.; Adams, F., Use of microscopic XRF for non-destructive analysis in art and archaeometry. *X-Ray Spectrometry: An International Journal* **2000,** *29* (1), 73-91.
2. Janssens, K. H., *Modern methods for analysing archaeological and historical glass*. John Wiley & Sons: 2013; Vol. 1.
3. Schalm, O.; Caen, J.; Janssens, K., Homogeneity, Composition and Deterioration of Window Glass Fragments and Paint Layers from Two Seventeenth-Century Stained Glass Windows Created by Jan de Caumont (~ 1580–1659). *Studies in conservation* **2010,** *55* (3), 216-226.
4. Adlington, L. W.; Freestone, I. C.; Kunicki-Goldfinger, J. J.; Ayers, T.; Gilderdale Scott, H.; Eavis, A., Regional patterns in medieval European glass composition as a provenancing tool. *Journal of Archaeological Science* **2019,** *110*, 104991.
5. Van der Snickt, G.; De Nolf, W.; Vekemans, B.; Janssens, K., μ-XRF/μ-RS vs. SR μ-XRPD for pigment identification in illuminated manuscripts. *Applied Physics A* **2008,** *92* (1), 59-68.
6. Janssens, K.; Alfeld, M.; Van der Snickt, G.; De Nolf, W.; Vanmeert, F.; Radepont, M.; Monico, L.; Dik, J.; Cotte, M.; Falkenberg, G., The use of synchrotron radiation for the characterization of artists' pigments and paintings. *Annual Review of Analytical Chemistry* **2013,** *6*, 399-425.
7. Legrand, S.; Van der Snickt, G.; Cagno, S.; Caen, J.; Janssens, K., MA-XRF imaging as a tool to characterize the 16th century heraldic stained-glass panels in Ghent Saint Bavo Cathedral. *Journal of Cultural Heritage* **2019,** *40*, 163-168.
8. Van der Snickt, G.; Legrand, S.; Caen, J.; Vanmeert, F.; Alfeld, M.; Janssens, K., Chemical imaging of stained-glass windows by means of macro X-ray fluorescence (MA-XRF) scanning. *Microchemical Journal* **2016,** *124*, 615-622.
9. Hunault, M.; Bauchau, F.; Loisel, C.; Hérold, M.; Galoisy, L.; Newville, M.; Calas, G., Spectroscopic Investigation of the Coloration and Fabrication Conditions of Medieval Blue Glasses. *Journal of the American Ceramic Society* **2016,** *99* (1), 89-97.
10. Capobianco, N.; Hunault, M. O. J. Y.; Balcon-Berry, S.; Galoisy, L.; Sandron, D.; Calas, G., The Grande Rose of the Reims Cathedral: an eight-century perspective on the colour management of medieval stained glass. *Scientific Reports* **2019,** *9* (1), 3287.
11. Colomban, P.; Tournié, A., On-site Raman identification and dating of ancient/modern stained glasses at the Sainte-Chapelle, Paris. *Journal of Cultural Heritage* **2007,** *8* (3), 242-256.
12. Bracci, S.; Bartolozzi, G.; Burnam, R. K.; Corallini, A., Integration of both non-invasive and micro-invasive techniques for the archaeometric study of the stained-glass window Apparizione degli Angeli in the basilica of Santa Croce in Florence, Italy. *Journal of Cultural Heritage* **2020,** *44*, 307-316.
13. Aulinas, M.; Garcia-Valles, M.; Gimeno, D.; Fernandez-Turiel, J. L.; Ruggieri, F.; Pugès, M., Weathering patinas on the medieval (S. XIV) stained glass windows of the Pedralbes Monastery (Barcelona, Spain). *Environmental Science and Pollution Research* **2009,** *16* (4), 443-452.
14. Pradell, T.; Molina, G.; Murcia, S.; Ibáñez, R.; Liu, C.; Molera, J.; Shortland, A. J., Materials, techniques, and conservation of historic stained glass "grisailles". *International Journal of Applied Glass Science* **2016,** *7* (1), 41-58.
15. Plaisier, J. R.; Nodari, L.; Gigli, L.; San Miguel, E. P. R.; Bertoncello, R.; Lausi, A., The X-ray diffraction beamline MCX at Elettra: a case study of non-destructive analysis on stained glass. *Acta Imeko* **2017,** *6* (3), 71-75.
16. García-Heras, M.; Gil, C.; Carmona, N.; Villegas, M., Weathering effects on materials from historical stained glass windows. *Materiales de Construcción* **2003,** *53* (270), 21-34.
17. Aubert, *Les vitraux de Notre-Dame et de la Sainte-Chapelle de Paris,*. Paris, 1959.
18. Perrot, F., Belgique. Anvers, un panneau de vitrail du Musée Mayer van Den Bergh provenant de la rose sud de Notre-Dame de Paris. *Bulletin Monumental* **1989**, 176-176.
19. Gatouillat, F., Les vitraux anciens, Notre-Dame de Paris, La grâce d'une cathédrale (Cardinal André Vingt-Trois ed.). La Nuée bleue/Place des Victoires: Paris, 2012; pp 64-65.
20. Helbig, J., *L'art du vitrail en Belgique*. 1969.
21. Alfeld, M.; Janssens, K.; Dik, J.; de Nolf, W.; van der Snickt, G., Optimization of mobile scanning macro-XRF systems for the in situ investigation of historical paintings. *Journal of Analytical Atomic Spectrometry* **2011,** *26* (5), 899-909.
22. Solé, V. A.; Papillon, E.; Cotte, M.; Walter, P.; Susini, J., A multiplatform code for the analysis of energy-dispersive X-ray fluorescence spectra. *Spectrochimica Acta Part B: Atomic Spectroscopy* **2007,** *62* (1), 63-68.
23. Alfeld, M.; Janssens, K., Strategies for processing mega-pixel X-ray fluorescence hyperspectral data: a case study on a version of Caravaggio's painting Supper at Emmaus. *Journal of analytical atomic spectrometry* **2015,** *30* (3), 777-789.
24. De Meyer, S.; Vanmeert, F.; Vertongen, R.; van Loon, A.; Gonzalez, V.; van der Snickt, G.; Vandivere, A.; Janssens, K., Imaging secondary reaction products at the surface of Vermeer's Girl with the Pearl Earring by means of macroscopic X-ray powder diffraction scanning. *Heritage Science* **2019,** *7* (1), 1-11.
25. De Nolf, W.; Vanmeert, F.; Janssens, K., XRPDUA: crystalline phase distribution maps by two-dimensional scanning and tomographic (micro) X-ray powder diffraction. *Journal of Applied Crystallography* **2014,** *47* (3), 1107-1117.
26. Sherman, J., The theoretical derivation of fluorescent X-ray intensities from mixtures. *Spectrochimica Acta* **1955,** *7*, 283-306.
27. Wedepohl, K. H.; Simon, K., The chemical composition of medieval wood ash glass from Central Europe. *Geochemistry* **2010,** *70* (1), 89-97.
28. Adlington, L. W.; Freestone, I. C., Using handheld pXRF to study medieval stained glass: A methodology using trace elements. *MRS Advances* **2017,** *2* (33-34), 1785-1800.
29. Dungworth, D., Historic windows: investigation of composition groups with nondestructive pXRF. *Glass Technology-European Journal of Glass Science and Technology Part A* **2012,** *53* (5), 192-197.
30. Schalm, O.; Janssens, K.; Wouters, H.; Caluwé, D., Composition of 12–18th century window glass in Belgium: Non-figurative windows in secular buildings and stained-glass windows in religious buildings. *Spectrochimica Acta Part B: Atomic Spectroscopy* **2007,** *62* (6-7), 663-668.
31. Frenzel, G., The restoration of medieval stained glass. *Scientific American* **1985,** *252* (5), 126-137.

32. Caviness, M. H., Three medallions of stained glass from the Sainte Chapelle of Paris. *Philadelphia Museum of Art Bulletin* **1967,** *62* (294), 245-259.
33. Kunicki-Goldfinger, J. J.; Freestone, I. C.; McDonald, I.; Hobot, J. A.; Gilderdale-Scott, H.; Ayers, T., Technology, production and chronology of red window glass in the medieval period – rediscovery of a lost technology. *Journal of Archaeological Science* **2014,** *41*, 89-105.
34. Weyl, W. A., Coloured glasses. In *Part of a collection of research on crystalline glazes donated (c. 1990) to CSAD by CI Brown. See Shelf 8, Boxes 5, 6, 7*, Society of glass technology: 1981.
35. Hunault, M. O.; Bauchau, F.; Boulanger, K.; Hérold, M.; Calas, G.; Lemasson, Q.; Pichon, L.; Pacheco, C.; Loisel, C., Thirteenth-century stained glass windows of the Sainte-Chapelle in Paris: An insight into medieval glazing work practices. *Journal of Archaeological Science: Reports* **2021,** *35*, 102753.
36. Hunault, M.; Calas, G.; Galoisy, L.; Lelong, G.; Newville, M., Local Ordering Around Tetrahedral Co2+ in Silicate Glasses. *Journal of the American Ceramic Society* **2014,** *97* (1), 60-62.
37. Kunicki-Goldfinger, J.; Kierzek, J.; Dzierzanowski, P.; Kasprzak, A. J., Central European crystal glass of the first half of the 18th century. **2005**.
38. Pérez-Villar, S.; Rubio, J.; Oteo, J. L., Study of color and structural changes in silver painted medieval glasses. *Journal of Non-Crystalline Solids* **2008,** *354* (17), 1833-1844.
39. Jembrih-Simbürger, D.; Neelmeijer, C.; Schalm, O.; Fredrickx, P.; Schreiner, M.; De Vis, K.; Mäder, M.; Schryvers, D.; Caen, J., The colour of silver stained glass—analytical investigations carried out with XRF, SEM/EDX, TEM, and IBA. *Journal of Analytical Atomic Spectrometry* **2002,** *17* (4), 321-328.
40. Schreurs, J. W.; Brill, R. H., Iron and sulfur related colors in ancient glasses. *Archaeometry* **1984,** *26* (2), 199-209.
41. Machado, C.; Vilarigues, M.; Palomar, T., Historical grisailles characterisation: A literature review. *Journal of Cultural Heritage* **2021**.
42. Carmona, N.; Villegas, M. A.; Navarro, J. M. F., Characterisation of an intermediate decay phenomenon of historical glasses. *Journal of Materials Science* **2006,** *41* (8), 2339-2346.
43. Adlington, L.; Freestone, I.; Seliger, L.; Martinon-Torres, M.; Brock, F.; Shortland, A., In situ methodology for compositional grouping of medieval stained glass windows. Cambridge Scholars Publishing: 2020.
44. Melcher, M.; Schreiner, M., Leaching studies on naturally weathered potash-lime–silica glasses. *Journal of Non-Crystalline Solids* **2006,** *352* (5), 368-379.
45. Schalm, O.; Nuyts, G.; Janssens, K., Some critical observations about the degradation of glass: The formation of lamellae explained. *Journal of Non-Crystalline Solids* **2021,** *569*, 120984.
46. Aulinas, M.; Garcia-Valles, M.; Gimeno, D.; Fernandez-Turiel, J. L.; Ruggieri, F.; Pugès, M., Weathering patinas on the medieval (S. XIV) stained glass windows of the Pedralbes Monastery (Barcelona, Spain). *Environmental Science and Pollution Research* **2008,** *16* (4), 443.
47. Piñar, G.; Garcia-Valles, M.; Gimeno-Torrente, D.; Fernandez-Turiel, J. L.; Ettenauer, J.; Sterflinger, K., Microscopic, chemical, and molecular-biological investigation of the decayed medieval stained window glasses of two Catalonian churches. *International Biodeterioration & Biodegradation* **2013,** *84*, 388-400.
48. Vilarigues, M.; Redol, P.; Machado, A.; Rodrigues, P. A.; Alves, L. C.; da Silva, R. C., Corrosion of 15th and early 16th century stained glass from the monastery of Batalha studied with external ion beam. *Materials Characterization* **2011,** *62* (2), 211-217.
49. Vilarigues, M.; da Silva, R. C., Ion beam and infrared analysis of medieval stained glass. *Applied Physics A* **2004,** *79* (2), 373-378.
50. Schalm, O.; Proost, K.; De Vis, K.; Cagno, S.; Janssens, K.; Mees, F.; Jacobs, P.; Caen, J., Manganese staining of archaeological glass: the characterization of Mn-rich inclusions in leached layers and a hypothesis of its formation. *Archaeometry* **2011,** *53* (1), 103-122.
51. Marschner, H. In *Analyses de pigments de grisaille sur des vitraux munichois de l'église du Saint-Sauveur, réalisés vers 1500*, Grisaille, jaune d'argent, sanguine, émail et peinture à froid: techniques et conservation. Forum pour la conservation et la restauration des vitraux, Liège, 19-22 juin 1996, 1996; pp 53-59.